materials

MDPI

Article

First Principles Investigation of Anomalous Pressure-Dependent Thermal Conductivity of Chalcopyrites

Loay Elalfy [1,*], Denis Music [1] and Ming Hu [2,*]

[1] Materials Chemistry, RWTH Aachen University, Kopernikusstr. 10, 52074 Aachen, Germany; Music@mch.rwth-aachen.de

[2] Department of Mechanical Engineering, University of South Carolina, Columbia, SC 29208, USA

* Correspondence: elalfy@mch.rwth-aachen.de (L.E.); hu@sc.edu (M.H.)

Received: 23 August 2019; Accepted: 23 October 2019; Published: 25 October 2019

Abstract: The effect of compression on the thermal conductivity of $CuGaS_2$, $CuInS_2$, $CuInTe_2$, and $AgInTe_2$ chalcopyrites (space group *I*-42*d*) was studied at 300 K using phonon Boltzmann transport equation (BTE) calculations. The thermal conductivity was evaluated by solving the BTE with harmonic and third-order interatomic force constants. The thermal conductivity of $CuGaS_2$ increases with pressure, which is a common behavior. Striking differences occur for the other three compounds. $CuInTe_2$ and $AgInTe_2$ exhibit a drop in the thermal conductivity upon increasing pressure, which is anomalous. $AgInTe_2$ reaches a very low thermal conductivity of 0.2 $W \cdot m^{-1} \cdot K^{-1}$ at 2.6 GPa, being beneficial for many energy devices, such as thermoelectrics. $CuInS_2$ is an intermediate case. Based on the phonon dispersion data, the phonon frequencies of the acoustic modes for $CuInTe_2$ and $AgInTe_2$ decrease with increasing pressure, thereby driving the anomaly, while there is no significant pressure effect for $CuGaS_2$. This leads to the negative Grüneisen parameter for $CuInTe_2$ and $AgInTe_2$, a decreased phonon relaxation time, and a decreased thermal conductivity. This softening of the acoustic modes upon compression is suggested to be due to a rotational motion of the chalcopyrite building blocks rather than a compressive oscillation. The negative Grüneisen parameters and the anomalous phonon behavior yield a negative thermal expansion coefficient at lower temperatures, based on the Grüneisen vibrational theory.

Keywords: thermal conductivity; pressure dependence; semiconductors; thermoelectric materials; chalcopyrites

1. Introduction

Chalcopyrite compounds ($A^IB^{III}C_2^{VI}$, A^I = IB elements (Cu, Ag), B^{III} = IIIA elements (Al, Ga, In), C^{VI} = VIA elements (S, Se, Te), space group *I*-42*d*, as shown in Figure 1) are well-known semiconductors with a band gap in the range of 0.1 to 1 eV [1–4]. The calculated band gap for the selected systems is 1.085, 0.364, 0.469, and 0.967 eV for $CuGaS_2$, $CuInS_2$, $AgInS_2$, and $AgInTe_2$, respectively [1–5], being consistent with common density functional theory deviations [6]. Their structure can be derived from zincblende (ZnS) by alternating the A^I and B^{III} constituents at the Zn site [7]. In the zincblende structure, a Zn atom is located in a center of a tetrahedron span by S, which is equivalent to an A^I- or B^{III}-based tetrahedron span by C^{VI} [7].

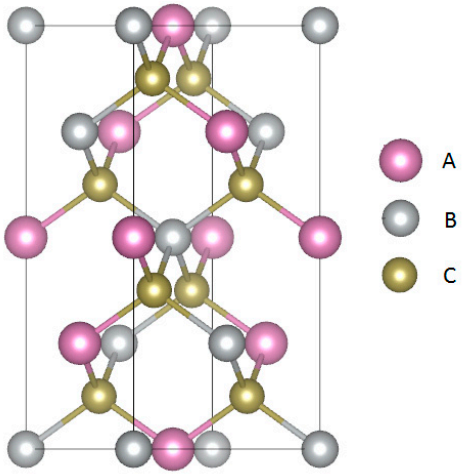

Figure 1. Crystal structure of the $A^{I}B^{III}C_2{}^{VI}$ chalcopyrite compounds.

These $A^{I}B^{III}C_2{}^{VI}$ compounds have been extensively studied for photovoltaic and thermoelectric applications [8–13]. The efficiency of thermoelectric devices depends on the thermoelectric figure of merit $ZT = TS^2\sigma/\kappa$, where T is the absolute temperature, S designates the Seebeck coefficient, σ is the electric conductivity, and κ stands for the thermal conductivity [14]. Other chalcopyrite compounds such as $CuFeS_2$ are currently under study for their mechanical, electronic, and thermodynamic properties, being promising for thermoelectric applications [15,16]. It is well established that κ decreases at elevated temperatures, which is beneficial for thermoelectric applications [17]. Different studies showed that pressure has an anomalous effect on $A^{II}B^{IV}$ zincblende compounds [18,19]. Using the Slack model, Gui et al. [2] showed that ZT of $CuInC_2{}^{VI}$ (C^{VI} = S, Se, and Te) uniformly increases at elevated temperatures up to 850 K. While the effect of pressure on κ and its relation to other thermal properties has been explored, the thermal expansion coefficient [20–22] has not been thoroughly studied. Furthermore, atomic vibrations driving anomalous thermal behavior of $CuInC_2{}^{VI}$ compounds are not known and cannot simply be deduced from other systems. Using the quasi-harmonic Debye model, Sharma et al. have evaluated electronic, thermal, and mechanical properties of $AgInC_2{}^{VI}$ (C^{VI} = S, Se, and Te) under pressure and reported a noticeable reduction in the Grüneisen parameter and volumetric thermal expansion coefficient, as well as the bulk modulus [23].

Since the Grüneisen parameter and volumetric thermal expansion coefficient can be related to κ (see below for more details), it appears that pressure effects on κ are considerable. This is consistent with an experimental study reporting a decrease in κ by 30% for $CuInTe_2$ under pressure up to 2.3 GPa [24]. Generally, κ should increase under compression [22]; however, the compounds in the current study exhibit a mixture of monotonic decrease and non-monotonic dependence under pressure. The latter phenomenon has been intensively studied recently [18,19,21]. This implies that the behavior of $CuInTe_2$ and related compounds is of great interest due to non-monotonicity. The behavior of $CuInTe_2$ is anomalous. Two possible mechanisms have been proposed based on experiments: (i) anharmonic behavior of lattice vibrations [24] and (ii) structural modifications under high pressure (e.g., stacking faults) [25]. The underlying physics of the κ reduction under compression of $CuInTe_2$, and possibly other $A^{I}B^{III}C_2{}^{VI}$ compounds, is not fully understood.

In this work, we devise a strategy to identify the physical origin of the anomalous behavior of κ of $A^{I}B^{III}C_2{}^{VI}$ compounds under compression. Using phonon calculations, the atomic-level understanding of this anomaly is obtained by analyzing the vibrational modes and correlating these to the macroscopic observables, such as κ. To systematically explore the pressure effect on κ, $CuInTe_2$ is taken as a reference, and the influence of mass, being decisive for lattice vibrations, is considered by replacing Cu with Ag, In with Ga, and Te with S within this isostructural and isoelectronic $A^{I}B^{III}C_2{}^{VI}$ system. Hence, $CuGaS_2$, $CuInS_2$, $CuInTe_2$, and $AgInTe_2$ chalcopyrites are explored.

2. Methods

In order to maximize ZT, σ and κ should be maximized and minimized, respectively. An increase in σ directly affects the total κ value, since $\kappa = \kappa_e + \kappa_{ph}$, where κ_e is the electronic thermal conductivity (charge carriers also conduct heat) and κ_{ph} is the lattice thermal conductivity. Hence, minimizing κ_{ph} is the major route to minimize the total κ value. Furthermore, κ_{ph} is likely the largest contribution for chalcopyrites since they are semiconductors. It can be obtained as follows: $\kappa_{ph} = \frac{1}{3} c_v v_g^2 \tau$, where v_g is the group velocity of phonons, c_v designates the heat capacity, and τ is the phonon relaxation time [26]. The former two values were calculated herein from the phonon dispersion curves using the Phonopy package [27], while τ was obtained by solving the Boltzmann transport equation, as implemented in the ShengBTE package [28]. The isotropic approximation was applied due to isotropic pressure dependence evaluated in the current study. Harmonic and third-order interatomic force constants within three coordination shells were used as input in both packages. All interatomic force constants were generated using the Vienna Ab-initio Simulation Package (VASP) [29–33]. The exchange-correlation functionals were treated within the local density approximation [34], including phonon calculations. The all-electron projector augmented wave method [35] was utilized to evaluate electronic wave functions with a plane wave cutoff of 800 eV and the total energy convergence of 10^{-7} eV. No configurations were spin polarized. All structures (internal free parameters) and unit cell sizes were optimized within a force convergence condition of 10^{-6} eV·Å^{-1}. A $4 \times 4 \times 2$ k-mesh Monkhorst-Pack [36] was used to sample the Brillouin zone (BZ) of the $2 \times 2 \times 1$ supercell (64 atoms) constructed from the conventional $A^{I}B^{III}C_2{}^{VI}$ unit cell (16 atoms, six coordination shells). Convergence tests were conducted for the k-mesh (from $2 \times 2 \times 1$ to $6 \times 6 \times 3$). At the chosen conditions ($4 \times 4 \times 2$), phonon band structure was converged and stable under pressure up to 9 GPa. Since a $10 \times 10 \times 10$ q-mesh leads to a fluctuation in κ_{ph} on the order of 10^{-1} W·m^{-1}·K^{-1} (348 atomic displacements per chalcopyrite configuration accumulating Hellmann–Feynman forces for the phonon calculations), such changes are acceptable for the calculated κ_{ph} values in the range of several W·m^{-1}·K^{-1}. As stated in the introduction, all $A^{I}B^{III}C_2{}^{VI}$ chalcopyrite compounds exhibit a band gap of >0.4 eV (see Table 1) so that only phonons are considered for the evaluation of the transport properties. The pressure dependence was modelled in the form of isotropic compressive strains in steps of 3% of the equilibrium unit cell volume (a minimum of 5 strains were considered per chalcopyrite configuration). The bulk moduli were calculated using the Rose–Vinet equation of state to evaluate the pressure associated with each strain [37]. The calculated bulk moduli for $CuGaS_2$, $CuInS_2$, $CuInTe_2$, and $AgInTe_2$ were 76.0, 64.6, 41.3, and 41.2 GPa, respectively, which is consistent with the literature [38–42] (see Table 1). The obtained lattice parameters were a = 5.387 Å and c/a = 1.981 for $CuGaS_2$, a = 5.597 Å and c/a = 2.015 for $CuInS_2$, a = 6.303 Å and c/a = 2.007 for $CuInTe_2$, and a = 6.582 Å and c/a = 1.978 for $AgInTe_2$. These lattice constants deviate max. 2.7% from the experimental data [43,44] (see Table 1), which is acceptable for the employed exchange-correlation functionals [6]. Finally, the quasi-harmonic approximation [45] was utilized to calculate the volumetric thermal expansion coefficient due to its relationship with κ_{ph}, as detailed below.

Table 1. Comparison between calculated and reported values for band gap, bulk modulus, lattice parameters, and thermal conductivity.

	Band Gap [1] (eV)		Bulk Modulus [2] (GPa)		Lattice Parameters [2] a (Å), c/a		κ [2] (W/mK)	
	This Work	Ref.	This Work	Ref.	This Work	Ref. [41]	This Work	Ref.
$CuGaS_2$	1.085	0.92 [1]	76.0	94 [39]	5.387, 1.981	5.34, 1.95	8.2	9.3 [46]
$CuInS_2$	0.364	0.35 [1]	64.6	75 [40]	5.597, 2.015	5.51, 2.00	4.6	-
$CuInTe_2$	0.469	0.02–0.91 [2]	41.3	45 [41]	6.303, 2.007	6.16, 2.00	2.9	2.7 [47]
$AgInTe_2$	0.976	0.91 [5]	41.2	41.1 [42]	6.582, 1.978	6.4, 1.96	7.6	6.2 [48]

[1] Band gaps are compared with computational results at 0 K, except for $AgInTe_2$. [2] Comparison with experimental values at room temperature.

3. Results and Discussion

3.1. Lattice Thermal Conductivity

In Figure 2, the lattice thermal conductivity of all $A^{I}B^{III}C_2{}^{VI}$ compounds studied in this work is plotted against an increasing pressure. First, the ambient pressure conditions (0 GPa) are discussed. $CuGaS_2$ exhibits a relatively large κ_{ph} value of 8.2 $W{\cdot}m^{-1}{\cdot}K^{-1}$, which deviates 12% from the measured one (9.3 $W{\cdot}m^{-1}{\cdot}K^{-1}$) [46]. In the case of $CuInS_2$, κ_{ph} reaches 4.6 $W{\cdot}m^{-1}{\cdot}K^{-1}$. The κ_{ph} value of $AgInTe_2$ is 2.9 $W{\cdot}m^{-1}{\cdot}K^{-1}$, which is only 7% offset from the experimental value of 2.7 $W{\cdot}m^{-1}{\cdot}K^{-1}$ [47]. $CuInTe_2$ attains 7.6 $W{\cdot}m^{-1}{\cdot}K^{-1}$, which is an 18% deviation compared to the experimentally obtained value of 6.2 $W{\cdot}m^{-1}{\cdot}K^{-1}$ [48]. Hence, these differences are acceptable based on the κ_{ph} deviations of other theoretical studies from measurements [46,49,50]. See Table 1 for comparison. Furthermore, based on a comparison of predicted and experimental κ_{ph} values for diamond, SiC, GaN, Si, GaAs, InSb, $SrTiO_3$, and PbTe, theoretical data at elevated temperatures commonly overestimate the measured values [51], so that the calculated low κ_{ph} data in this study should be even lower under ordinary experimental conditions (e.g., presence of defects). It is clear that trends are properly captured within the methodology used in the current study.

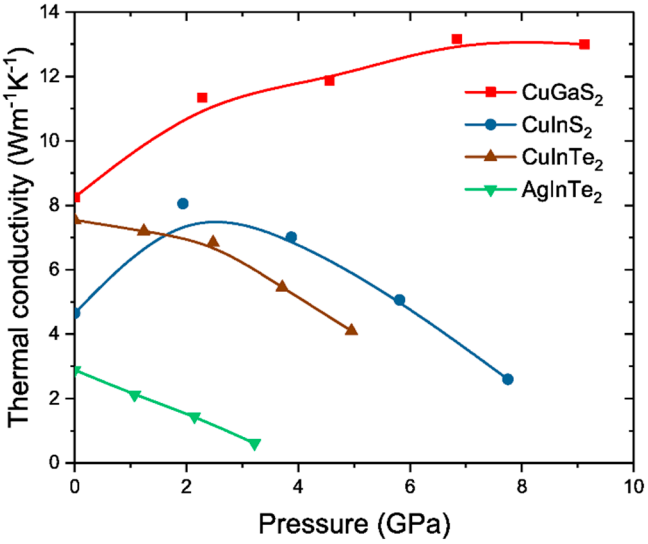

Figure 2. Thermal conductivity at 300 K for $CuGaS_2$, $CuInS_2$, $CuInTe_2$, and $AgInTe_2$ under compression. The solid lines connecting the data points serve as a guide to the eye.

Striking differences were obtained between the κ_{ph} behavior of $CuGaS_2$, $CuInS_2$, $CuInTe_2$, and $AgInTe_2$ under compression (see Figure 2). The pressure range explored herein can be reached in samples synthesized by non-equilibrium vapor phase condensation processes [52]. The κ_{ph} value of $CuGaS_2$ always increases with pressure up to 9.5 GPa. This is a common behavior for most compounds [22]. A drastically different dependence is obtained as soon as the heavier In is considered instead of Ga (B^{III} in $A^{I}B^{III}C_2{}^{VI}$). Under pressure up to 6 GPa, the κ_{ph} of $CuInTe_2$ decreases from 7.6 to 4.1 $W{\cdot}m^{-1}{\cdot}K^{-1}$, which is anomalous. This is consistent with the experimental data [24,25], implying that important physics is captured within the methodology employed herein and structural modulations are not indispensable to drive the anomaly. By exchanging Te with lighter S (C^{VI} in $A^{I}B^{III}C_2{}^{VI}$) and hence forming $CuInS_2$, κ_{ph} increases up to 2 GPa, which is again a common behavior and equivalent to that of $CuGaS_2$. Upon a further pressure increase, κ_{ph} begins to decrease and reaches a slightly lower value at 8 GPa than that at 0 GPa. To account for the effect of the transition metal constituent (A^{I} in $A^{I}B^{III}C_2{}^{VI}$), Cu in $CuInTe_2$ is exchanged with the heavier Ag. $AgInTe_2$ exhibits a significantly lower κ_{ph} value and a steeper decrease in κ_{ph} under pressure, reaching 0.2 $W{\cdot}m^{-1}{\cdot}K^{-1}$ at 2.6 GPa. This is a very low value for κ_{ph} and is comparable to that of some polymers, such as polytetrafluoroethylene [53].

Such low κ_{ph} values under pressure should lead to an enhanced thermoelectric performance, according to several studies [54–56].

3.2. Acoustic Phonon Dispersion

Since κ_{ph} and all the corresponding factors, v_g, c_v, and τ, are governed by phonons, phonon dispersion curves are further discussed to explain the anomalous behavior. The acoustic phonon modes at 300 K contribute 85%, 70%, 60%, and 80% of κ_{ph} for $CuGaS_2$, $CuInS_2$, $CuInTe_2$, and $AgInTe_2$, respectively, so that non-locality of the exchange-correlation functional is of less significance since it would mainly contribute to optical phonon frequencies [57]. Therefore, in this study, the behavior of acoustic phonon modes and the effect of pressure thereon are considered in detail. Since $AgInTe_2$ and $CuInTe_2$ exhibit the same κ_{ph} behavior, whereby the former undergoes a more drastic change, $AgInTe_2$ is taken as a representative. Figure 3 contains the acoustic phonon modes under different pressures for $CuGaS_2$ (common κ_{ph} behavior), $CuInS_2$ (intermediate case), and $AgInTe_2$ (anomalous case). The effect of pressure on the phonon dispersion curves for different compounds is noticeably different. For $CuGaS_2$ (Figure 3a), all acoustic transverse (TA) and longitudinal (LA) modes are not significantly affected by pressure. In the case of $AgInTe_2$ (Figure 3c), the phonon modes are considerably softened over the entire BZ. The phonon modes of $CuInS_2$ (Figure 3b) do not behave uniformly. The TA modes of $CuInS_2$ are similar to the behavior of $AgInTe_2$ after crossing a pressure threshold, and the LA modes are more like those of $CuGaS_2$.

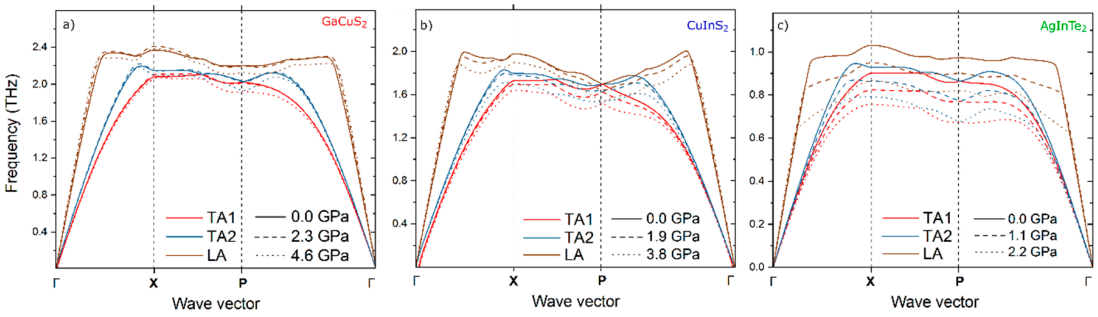

Figure 3. Acoustic phonon dispersion at different pressures of (**a**) $CuGaS_2$, (**b**) $CuInS_2$, and (**c**) $AgInTe_2$. TA1 and TA2 are two transverse acoustic modes, and LA is a longitudinal acoustic mode.

The atomic vibrations were analyzed from the phonon dispersion curves using a tool developed by Miranda et al. [58]. For the phonon modes with decreasing frequency upon compression, e.g., LA of $AgInTe_2$ starting at (0, 0, 0.3) on the Γ-X and X-P path (30% of the path length), as shown in Figure 3c, the vibrations are unconventional. The metal-centered tetrahedra (A^I in $A^IB^{III}C_2{}^{VI}$) oscillate in the manner that the angles between neighboring units are changing, while the bond lengths are fixed. However, the conventional thermal vibrations occur in the form of a compression wave, where the bonds are mostly stretched, as in the case of $CuGaS_2$. The anomalous behavior is due to the circular motion of the metal atoms (A^I = Cu or Ag) around the equilibrium position. The anomalous chalcopyrites tend to keep the bond length fixed and the excitations appear in the form of bond bending. Such behavior is consistent with the tension effect introduced by Dove et al. [59], showing that in the case where the energy required for stretching is too high, a finite transverse displacement in the centers of polyhedra occurs, resulting in rotation.

3.3. Phonon Relaxation Time

A decrease in the phonon frequency upon compression (softening of the acoustic phonon modes) implies the negative Grüneisen parameter (γ), which can be related to τ ($1/\tau = \gamma^2$ within the Debye–Callaway model [60]) one of the three physical variables describing κ_{ph}. Since ${v_g}^2$ decreases uniformly with pressure for all $A^{I}B^{III}{C_2}^{VI}$ compounds explored in this work and c_v is affected by only 0.1%, it appears that τ is the major constituent responsible for the anomaly. Hence, τ is further explored for $CuGaS_2$, $CuInS_2$, and $AgInTe_2$ as a function of pressure. The corresponding τ data for the acoustic phonon modes are shown in Figure 4. For $CuGaS_2$ (Figure 4a), τ increases up to 300% with pressure. This implies that the absolute value of γ decreases. For $CuInS_2$ (Figure 4b), τ increases up to 2 GPa in the case of TA and further to 4 GPa in the case of LA and TAs and then decreases, which is supported by the fact that γ changes the sign for a number of low-frequency phonons as appearing in the dispersion relation in Figure 3b. For $AgInTe_2$ (Figure 4c), τ decreases in the whole pressure range and hence γ^2 is increasing, while the values are negative (softening of the acoustic phonon modes). Therefore, an increasing τ with pressure gives rise to an increasing κ_{ph}, as in the case of $CuGaS_2$. Anomalous κ_{ph} of $AgInTe_2$ exhibits a small τ value and negative γ. The notion of negative γ values and softening of the acoustic phonon modes is consistent with the literature on $AgGaS_2$ [61]. In the present work, an important step is made towards a relationship with κ_{ph}.

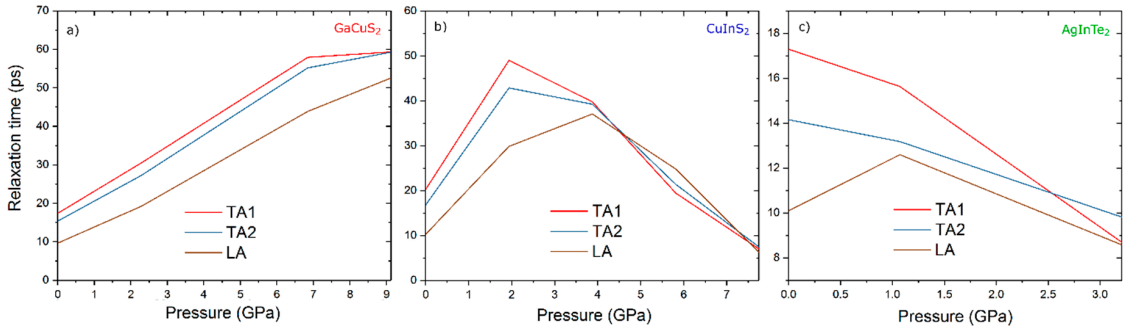

Figure 4. Phonon relaxation time under pressure of (**a**) $CuGaS_2$, (**b**) $CuInS_2$, and (**c**) $AgInTe_2$. TA1 and TA2 are two transverse acoustic modes, and LA is a longitudinal acoustic mode.

3.4. Thermal Expansion Coeficient

According to the Grüneisen vibrational theory of thermal expansion [59], negative γ yields a negative volumetric thermal expansion coefficient (α) since $\gamma = \alpha V / Bc_v$, where V is the volume and B stands for the bulk modulus. As α can be obtained independently from γ (quasi-harmonic approximation was used herein), probing α is important. Furthermore, this may help other experimentalists, besides those focusing on thermoelectric devices, to critically appraise the results obtained in this study. Therefore, in Figure 5 the α value is plotted at different temperatures. For $CuGaS_2$, having an increasing κ_{ph} value under pressure, α is always positive. $CuInS_2$ possesses a slightly negative α value. However, both $CuInTe_2$ and $AgInTe_2$ exhibit negative α at low temperatures. The pressure dependence on α is not shown here since the major effect is an offset of the negative α region to higher temperatures, conserving the trends between these chalcopyrites. The anomalous behavior of $CuInTe_2$ and $AgInTe_2$ is thus driven by softening of the acoustic phonon modes under compression, leading to negative α and γ.

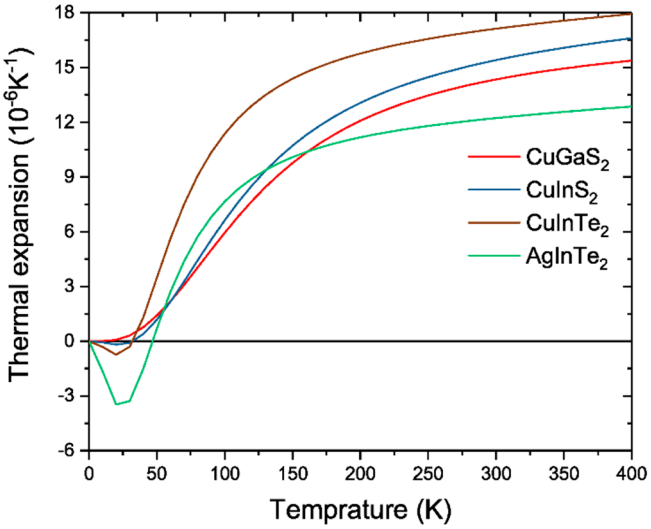

Figure 5. Volumetric thermal expansion coefficient at ambient pressure for $CuGaS_2$, $CuInS_2$, $CuInTe_2$, and $AgInTe_2$.

4. Conclusions

The thermal conductivity of $CuGaS_2$, $CuInS_2$, $CuInTe_2$, and $AgInTe_2$ $A^IB^{III}C_2{}^{VI}$ chalcopyrites exhibits a different behavior under pressure, ranging from increasing ($CuGaS_2$), as for most compounds, alternating (increasing and decreasing for $CuInS_2$), and to decreasing, as in the case for $CuInTe_2$ and $AgInTe_2$, which is anomalous. This can be understood based on the phonon dispersion curves. Softening of the acoustic phonon modes occurs for these anomalous chalcopyrites. This leads to the negative Grüneisen parameter and negative volumetric thermal expansion coefficient. The decrease in phonon frequency upon compression is suggested to be due to the phonon oscillations in the form of a rotational motion rather than compressive waves. The physical origin of the anomalous thermal conductivity is thus identified in this work in terms of higher-order phonon—phonon interactions, and $AgInTe_2$ with a very low thermal conductivity of 0.2 $W{\cdot}m^{-1}{\cdot}K^{-1}$ at 2.6 GPa is proposed to be a promising thermoelectric compound.

Author Contributions: L.E., D.M., and M.H. contributed to the conceptualization of this paper. The methodology and the software used were proposed by M.H., and specific parameters were chosen by L.E. Analysis and investigations were carried out by L.E. with the support of other authors. The paper was written by L.E., with contributions from the other two authors. M.H. was responsible for acquiring funding.

Funding: This work was supported by the Deutsche Forschungsgemeinschaft (DFG) within the project HU 2269/10. Simulations were performed with computing resources granted by JARA-HPC from RWTH Aachen University under project JARA0131. Research reported in this publication was supported in part by the NSF and SC EPSCoR/IDeA Program under award number (NSF Award #OIA-1655740 via SC EPSCoR/IDeA GEAR-CRP2019 19-GC02). The views, perspective, and content do not necessarily represent the official views of the SC EPSCoR/IDeA Program nor those of the NSF.

Conflicts of Interest: The authors declare no conflict of interest.

References

1. Rashkeev, S.N.; Lambrecht, W.R.L. Second-harmonic generation of I-III-VI2 chalcopyrite semiconductors: Effects of chemical substitutions. *Phys. Rev. B* **2001**, *63*, 165212. [CrossRef]
2. Gui, Y.; Ye, L.; Jin, C.; Zhang, J.; Wang, Y. The nature of the high thermoelectric properties of $CuInX_2$ (X = S, Se and Te): First-principles study. *Appl. Surf. Sci.* **2018**, *458*, 564–571. [CrossRef]
3. Zou, D.; Xie, S.; Liu, Y.; Lin, J.; Li, J. First-principles study of thermoelectric and lattice vibrational properties of chalcopyrite $CuGaTe_2$. *J. Alloy. Compd.* **2013**, *570*, 150–155. [CrossRef]
4. Xu, B.; Li, X.; Qin, Z.; Long, C.; Yang, D.; Sun, J.; Yi, L. Electronic and optical properties of $CuGaS_2$: First-principles calculations. *Phys. B Condens. Matter* **2011**, *406*, 946–951. [CrossRef]

5. Bellabarba, C.; Ganzáles, J.; Rincon, C.; Quintero, M. Photoconductivity and valence band structure of $AgInTe_2$. *Solid State Commun.* **1986**, *58*, 243–246. [CrossRef]
6. Paier, J.; Marsman, M.; Hümmer, K.; Kresse, G.; Gerber, I.C.; Ángyán, J.G. Screened hybrid density functionals applied to solids. *J. Chem. Phys.* **2006**, *124*, 154709. [CrossRef]
7. Yan, B.; Zhang, S.-C. Topological materials. *Rep. Prog. Phys.* **2012**, *75*, 96501. [CrossRef]
8. Ramanujam, J.; Singh, U.P. Copper indium gallium selenide based solar cells—A review. *Energy Environ. Sci.* **2017**, *10*, 1306–1319. [CrossRef]
9. Yao, J.; Takas, N.J.; Schliefert, M.L.; Paprocki, D.S.; Blanchard, P.E.R.; Gou, H.; Mar, A.; Exstrom, C.L.; Darveau, S.A.; Poudeu, P.F.P.; et al. Thermoelectric properties of p-type $CuInSe_2$ chalcopyrites enhanced by introduction of manganese. *Phys. Rev. B* **2011**, *84*, 075203. [CrossRef]
10. Shi, X.; Xi, L.; Fan, J.; Zhang, W.; Chen, L. Cu–Se Bond Network and Thermoelectric Compounds with Complex Diamondlike Structure. *Chem. Mater.* **2010**, *22*, 6029–6031. [CrossRef]
11. Gudelli, V.K.; Kanchana, V.; Vaitheeswaran, G.; Svane, A.; Christensen, N.E. Thermoelectric properties of chalcopyrite type $CuGaTe_2$ and chalcostibite $CuSbS_2$. *J. Appl. Phys.* **2013**, *114*, 223707. [CrossRef]
12. He, J.; Tritt, T.M. Advances in thermoelectric materials research: Looking back and moving forward. *Science* **2017**, *357*, eaak9997. [CrossRef] [PubMed]
13. Lu, Y.; Chen, S.; Wu, W.; Du, Z.; Chao, Y.; Cui, J. Enhanced thermoelectric performance of a chalcopyrite compound $CuIn_3Se_{5-x}Te_x$ (x = 0~0.5) through crystal structure engineering. *Sci. Rep.* **2017**, *7*, 40224. [CrossRef] [PubMed]
14. Disalvo, F.J. Thermoelectric Cooling and Power Generation. *Science* **1999**, *285*, 703–706. [CrossRef] [PubMed]
15. Khalediali dusti, R.; Mishra, A.K.; Barnoush, A. Temperature-dependent properties of magnetic $CuFeS_2$ from first-principles calculations: Structure, mechanics, and thermodynamics. *AIP Adv.* **2019**, *9*, 065021. [CrossRef]
16. Park, J.; Xia, Y.; Ozoliņš, V. First-principles assessment of thermoelectric properties of $CuFeS_2$. *J. Appl. Phys.* **2019**, *125*, 125102. [CrossRef]
17. Holland, M.G. Phonon Scattering in Semiconductors from Thermal Conductivity Studies. *Phys. Rev.* **1964**, *134*, A471–A480. [CrossRef]
18. Ouyang, T.; Hu, M. Competing mechanism driving diverse pressure dependence of thermal conductivity of XTe (X = Hg, Cd, and Zn). *Phys. Rev. B* **2015**, *92*, 235204. [CrossRef]
19. Yuan, K.; Zhang, X.; Tang, D.; Hu, M. Anomalous pressure effect on the thermal conductivity of ZnO, GaN, and AlN from first-principles calculations. *Phys. Rev. B* **2018**, *98*, 144303. [CrossRef]
20. Slack, G.A.; Andersson, P. Pressure and temperature effects on the thermal conductivity of CuCl. *Phys. Rev. B* **1982**, *26*, 1873–1884. [CrossRef]
21. Ravichandran, N.K.; Broido, D. Non-monotonic pressure dependence of the thermal conductivity of boron arsenide. *Nat. Commun.* **2019**, *10*, 827. [CrossRef] [PubMed]
22. Hofmeister, A.M. Pressure Dependence of Thermal Transport Properties. *Proc. Natl. Acad. Sci. USA* **2007**, *104*, 9192–9197. [CrossRef] [PubMed]
23. Sharma, S.; Verma, A.; Jindal, V. First principles studies of structural, electronic, optical, elastic and thermal properties of Ag-chalcopyrites ($AgInX_2$: X = S, Se). *Phys. B Condens. Matter* **2014**, *438*, 97–108. [CrossRef]
24. Yu, H.; Chen, L.-C.; Pang, H.-J.; Qin, X.-Y.; Qiu, P.-F.; Shi, X.; Chen, L.-D.; Chen, X.-J. Large enhancement of thermoelectric performance in $CuInTe_2$ upon compression. *Mater. Today Phys.* **2018**, *5*, 1–6. [CrossRef]
25. Kosuga, A.; Umekage, K.; Matsuzawa, M.; Sakamoto, Y.; Yamada, I. Room-Temperature Pressure-Induced Nanostructural $CuInTe_2$ Thermoelectric Material with Low Thermal Conductivity. *Inorg. Chem.* **2014**, *53*, 6844–6849. [CrossRef] [PubMed]
26. Omini, M.; Sparavigna, A.C. Beyond the isotropic-model approximation in the theory of thermal conductivity. *Phys. Rev. B* **1996**, *53*, 9064–9073. [CrossRef]
27. Togo, A.; Tanaka, I. First principles phonon calculations in materials science. *Scr. Mater.* **2015**, *108*, 1–5. [CrossRef]
28. Li, W.; Carrete, J.; Katcho, N.A.; Mingo, N. ShengBTE: A solver of the Boltzmann transport equation for phonons. *Comput. Phys. Commun.* **2014**, *185*, 1747–1758. [CrossRef]
29. Kresse, G.; Furthmüller, J. Efficient iterative schemes for ab initio total-energy calculations using a plane-wave basis set. *Phys. Rev. B* **1996**, *54*, 11169–11186. [CrossRef]

30. Kresse, G.; Furthmüller, J. Efficiency of ab-initio total energy calculations for metals and semiconductors using a plane-wave basis set. *Comput. Mater. Sci.* **1996**, *6*, 15–50. [CrossRef]
31. Kresse, G.; Hafner, J. Ab initio molecular dynamics for liquid metals. *Phys. Rev. B* **1993**, *47*, 558–561. [CrossRef] [PubMed]
32. Kresse, G.; Hafner, J. Ab initio molecular-dynamics simulation of the liquid-metal–amorphous-semiconductor transition in germanium. *Phys. Rev. B* **1994**, *49*, 14251–14269. [CrossRef] [PubMed]
33. Kresse, G.; Joubert, D. From ultrasoft pseudopotentials to the projector augmented-wave method. *Phys. Rev. B* **1999**, *59*, 1758–1775. [CrossRef]
34. Perdew, J.P.; Zunger, A. Self-interaction correction to density-functional approximations for many-electron systems. *Phys. Rev. B* **1981**, *23*, 5048–5079. [CrossRef]
35. Blöchl, P.E. Projector augmented-wave method. *Phys. Rev. B* **1994**, *50*, 17953–17979. [CrossRef] [PubMed]
36. Monkhorst, H.J.; Pack, J.D. Special points for Brillouin-zone integrations. *Phys. Rev. B* **1976**, *13*, 5188–5192. [CrossRef]
37. Vinet, P.; Smith, J.R.; Ferrante, J.; Rose, J.H. Temperature effects on the universal equation of state of solids. *Phys. Rev. B* **1987**, *35*, 1945–1953. [CrossRef]
38. Meng, Q.-B.; Xiao, C.-Y.; Wu, Z.-J.; Feng, K.-A.; Lin, Z.-D.; Zhang, S.-Y. Bulk modulus of ternary chalcopyrite AIBIIIC2VI and AIIBIVC2V semiconductors. *Solid State Commun.* **1998**, *107*, 369–371. [CrossRef]
39. Bettini, M.; Holzapfel, W. Grüneisen parameters of τ phonons in $CdSiP_2$, $CuAlS_2$ and $CuGaS_2$. *Solid State Commun.* **1975**, *16*, 27–30. [CrossRef]
40. Rincón, C.; Villareal, I.; Galindo, H. Microhardness-bulk modulus scaling and pressure-induced phase transformations in $A^IB^{III}C_2^{VI}$ chalcopyrite compounds. *J. Appl. Phys.* **1999**, *86*, 2355–2357. [CrossRef]
41. Fernandez, B.; Wasim, S.M. Sound Velocities and Elastic Moduli in $CuInTe_2$ and $CuInSe_2$. *Phys. Status solidi (A)* **1990**, *122*, 235–242. [CrossRef]
42. Deus, P.; Schneider, H.A. A simple estimation of the bulk module of ternary chalcopyrite semiconducting compounds by means of the debye characteristic temperature. *Cryst. Res. Technol.* **1985**, *20*, 867–869. [CrossRef]
43. Madelung, O.; Rössler, U.; Schulz, M. (Eds.) I-III-VI2 Compounds Impurity, Lattice, Transport and Optical Properties: Comparative Data. In *Ternary Compounds, Organic Semiconductors*; Springer: Berlin/Heidelberg, Germany, 2000; pp. 1–7.
44. Hahn, H.; Frank, G.; Klingler, W.; Meyer, A.-D.; Störger, G. Untersuchungen über ternäre Chalkogenide. V. Über einige ternäre Chalkogenide mit Chalkopyritstruktur. *Z. Anorg. Allg. Chem.* **1953**, *271*, 153–170. [CrossRef]
45. Togo, A.; Chaput, L.; Tanaka, I.; Hug, G. First-principles phonon calculations of thermal expansion in Ti_3SiC_2, Ti_3AlC_2, and Ti_3GeC_2. *Phys. Rev. B* **2010**, *81*, 174301. [CrossRef]
46. Shibuya, T.; Skelton, J.M.; Jackson, A.J.; Yasuoka, K.; Togo, A.; Tanaka, I.; Walsh, A. Suppression of lattice thermal conductivity by mass-conserving cation mutation in multi-component semiconductors. *APL Mater.* **2016**, *4*, 104809. [CrossRef]
47. Charoenphakdee, A.; Kurosaki, K.; Muta, H.; Uno, M.; Yamanaka, S. Thermal Conductivity of the Ternary Compounds: $AgMTe_2$ and AgM_5Te_8 (M = Ga or In). *Mater. Trans.* **2009**, *50*, 1603–1606. [CrossRef]
48. Liu, R.; Xi, L.; Liu, H.; Shi, X.; Zhang, W.; Chen, L. Ternary compound $CuInTe_2$: A promising thermoelectric material with diamond-like structure. *Chem. Commun.* **2012**, *48*, 3818–3820. [CrossRef]
49. Kistaiah, P.; Murthy, K.S.; Iyengar, L. Correlation Between the Structural Parameters and the Thermal Conductivity of Chalcopyrite-Type Ternary Compounds. In *Thermal Conductivity 18*; Ashworth, T.S.D.R., Ed.; Springer: Berlin, Germany, 1985; pp. 127–137.
50. Rincon, C.; Wasim, S.M.; Valeri-Gil, M.L.; Valeri-Gil, M.L. Room-Temperature Thermal Conductivity and Grüneisen Parameter of the I–III–VI2 Chalcopyrite Compounds. *Phys. Status solidi (A)* **1995**, *147*, 409–415. [CrossRef]
51. McGaughey, A.J.H.; Jain, A.; Kim, H.-Y.; Fu, B. Phonon properties and thermal conductivity from first principles, lattice dynamics, and the Boltzmann transport equation. *J. Appl. Phys.* **2019**, *125*, 011101. [CrossRef]
52. Janssen, G.C.A.M.; Kamminga, J.-D. Stress in hard metal films. *Appl. Phys. Lett.* **2004**, *85*, 3086–3088. [CrossRef]

53. Blumm, J.; Lindemann, A.; Meyer, M.; Strasser, C. Characterization of PTFE Using Advanced Thermal Analysis Techniques. *Int. J. Thermophys.* **2010**, *31*, 1919–1927. [CrossRef]
54. Zou, D.; Yu, C.; Li, Y.; Ou, Y.; Gao, Y. Pressure-induced enhancement in the thermoelectric properties of monolayer and bilayer $SnSe_2$. *R. Soc. Open Sci.* **2018**, *5*, 171827. [CrossRef] [PubMed]
55. Bourassa, R.R.; Lazarus, D.; Blackburn, D.A. Effect of High Pressure on the Thermoelectric Power and Electrical Resistance of Aluminum and Gold. *Phys. Rev.* **1968**, *165*, 853–864. [CrossRef]
56. Zhang, Y.; Jia, X.; Sun, H.; Sun, B.; Liu, B.; Liu, H.; Kong, L.; Ma, H. Effect of high pressure on thermoelectric performance and electronic structure of SnSe via HPHT. *J. Alloys. Compd.* **2016**, *667*, 123–129. [CrossRef]
57. Lindsay, L.; Hua, C.; Ruan, X.; Lee, S. Survey of ab initio phonon thermal transport. *Mater. Today Phys.* **2018**, *7*, 106–120. [CrossRef]
58. Miranda, H.P.C.; Reichardt, S.; Froehlicher, G.; Molina-Sánchez, A.; Berciaud, S.; Wirtz, L. Quantum Interference Effects in Resonant Raman Spectroscopy of Single- and Triple-Layer $MoTe_2$ from First-Principles. *Nano Lett.* **2017**, *17*, 2381–2388. [CrossRef]
59. Dove, M.T.; Fang, H. Negative thermal expansion and associated anomalous physical properties: Review of the lattice dynamics theoretical foundation. *Rep. Prog. Phys.* **2016**, *79*, 66503. [CrossRef]
60. Callaway, J. Model for Lattice Thermal Conductivity at Low Temperatures. *Phys. Rev.* **1959**, *113*, 1046–1051. [CrossRef]
61. Yang, J.; Fan, Q.; Yu, Y.; Zhang, W. Pressure Effect of the Vibrational and Thermodynamic Properties of Chalcopyrite-Type Compound $AgGaS_2$: A First-Principles Investigation. *Materials* **2018**, *11*, 2370. [CrossRef]